

Mobility edges through inverted quantum many-body scarring

N. S. Srivatsa,^{1,2,3} Hadi Yarloo,⁴ Roderich Moessner,³ and Anne E. B. Nielsen⁴

¹*Department of Physics, King's College London, Strand WC2R 2LS, UK*

²*School of Physics and Astronomy, University of Birmingham, Birmingham, B15 2TT, UK*

³*Max-Planck-Institut für Physik komplexer Systeme, D-01187 Dresden, Germany*

⁴*Department of Physics and Astronomy, Aarhus University, DK-8000 Aarhus C, Denmark*

We show that the rainbow state, which has volume law entanglement entropy for most choices of bipartitions, can be embedded in a many-body localized spectrum. For a broad range of disorder strengths in the resulting model, we numerically find a narrow window of highly entangled states in the spectrum, embedded in a sea of area law entangled states. The construction hence embeds mobility edges in many-body localized systems. This can be thought of as the complement to many-body scars, an ‘inverted quantum many-body scar’, providing a further type of setting where the eigenstate thermalization hypothesis is violated.

When physical systems thermalize, most of the information about their initial state is lost. In the context of quantum mechanics, thermalization is explained through the eigenstate thermalization hypothesis [1, 2], which essentially states that an eigenstate encodes thermodynamic observables characteristic of its energy density. Settings in which quantum systems violate the eigenstate thermalization hypothesis are presently attracting much attention, both for understanding the foundations of many-body physics, and for utilizing their unusual properties, possibly even to store and control the flow of quantum information [3].

The entanglement entropy of states in the bulk of the spectrum of thermalizing quantum many-body systems is expected to scale with the volume of the system [4, 5]. Strong disorder, however, affects all states in the spectrum through the mechanism of many-body localization (MBL) inducing area-law entanglement in the eigenstates and hence nonthermal behavior [6]. MBL turns out to be a fragile phenomenon in the sense that there is no agreement of whether it persists beyond a (possibly very long) prethermal timescale [7–9]. The regime of finite systems and finite time scales is, however, by itself interesting and relevant for current experiments [10].

A weaker violation of the eigenstate thermalization hypothesis occurs in systems with quantum many-body scars [11–13]. Conventionally, scarred states are weakly entangled with subthermal scaling of the entanglement entropy [14–20], and procedures to embed these special states in the bulk of an otherwise thermal spectrum have been developed [21].

These studies raise the question, whether one can also have the converse situation, namely volume law entangled states embedded in a spectrum of MBL states, which we will refer to as inverted quantum many-body scars. Constructing such a model would lead to a different type of nonthermal system beyond MBL and quantum many-body scars. The construction is also interesting from the point of view of mobility edges in MBL. A mobility edge separates localized from delocalized states as a function of energy density, and its existence in the thermodynamic limit, as a matter of principle, is also in question [22–25].

First steps toward constructing inverted quantum many-body scars were taken in [26, 27], where a critical state with logarithmic scaling of the entanglement entropy was embedded in an MBL spectrum, albeit in a model with a highly non-local Hamiltonian and a state with sub-volume law entanglement. A simpler, but still non-local, Hamiltonian was also proposed, but for that case the embedded state was the ground state or a low-lying excited state.

In this paper, we present a local Hamiltonian that allows us to embed a volume law state inside an MBL spectrum. The volume law state is an exact eigenstate for all disorder realizations and hence remains intact even for strong disorder. We specifically consider the rainbow state, which has volume law entanglement for almost all bipartitions. This state is also referred to as an infinite temperature thermofield state [28].

In quantum many-body scar models, it is quite common that states with energies close to a scar state also have lower entanglement than the thermal part of the spectrum [15, 29, 30]. Here, we similarly find that states in the immediate vicinity of the inverted scar state have higher entropy than the MBL states. The number of high entropy states scales exponentially with system size, but with a small enough exponent that the number of high entropy states has measure zero in the large system limit.

The high entropy states produce mobility edges in the localized spectrum. While mobility edges have been observed numerically at the transition from thermal to MBL behavior in several moderate size systems [31], the mobility edges produced by inverted scars are different, as they occur over a broad range of disorder strengths and are particularly sharp as a function of energy density. These properties may be appealing for experimental investigations and practical utilization.

It is well-known that Anderson localized single-particle spectra of non-interacting systems can contain a few delocalized states, as happens, e.g., in quantum Hall systems, when interactions can be neglected [32]. The model presented here differs from that phenomenon in several ways. First, we are here considering a strongly interacting system, and the delocalized states appear in the

middle of the *many-particle* spectrum, while the quantum Hall effects happen at low temperature. Second, the rainbow state is volume law entangled, while the delocalized quantum Hall states are less entangled. Third, the quantum Hall effects are eventually destroyed by strong disorder, while in our case the rainbow state is immune to the added disorder.

The model that we investigate also raises interesting questions from a fundamental perspective. The model is generic, except that the disorder must fulfil a particular mirror symmetry. As long as this symmetry is obeyed, the volume law eigenstate persists for all disorder strengths and system sizes. It is well-known that symmetry can lead to delocalization [33–35]. The special property here is that the symmetry only produces a narrow window of delocalized states rather than delocalizing the entire spectrum. As is generally the case for MBL systems, our finite size numerics is not capable of judging whether the disorder strength at which the transition to MBL takes place remains finite in the thermodynamic limit. If MBL persists in the thermodynamic limit, we expect our (symmetry protected) mobility edges to do likewise.

Finally, we investigate what happens if the mirror symmetry is broken. For a particular system size and disorder strength, we find the inverted scarring to be quite fragile, disappearing already for an admixture of about 0.3% of non-symmetric disorder.

Model—The starting point for our construction of an inverted quantum many-body scar is the so-called rainbow model [36–38] for a chain of $2N$ sites. Here, we consider the general rainbow Hamiltonian

$$H = H_1 \otimes I - I \otimes H_2 + c V_{\text{int}} \quad (1)$$

proposed in [39]. H_1 acts on the sites 1 to N , and H_2 acts on the sites $N+1$ to $2N$. $H_2 = M H_1^* M$, where M is the mirror operation that maps site i into site $2N+1-i$, and the complex conjugation is performed in a chosen product state basis. We shall here consider spin-1/2 particles with

$$H_1 = \sum_{i=1}^{N-1} (J_x S_i^x S_{i+1}^x + J_y S_i^y S_{i+1}^y + J_z S_i^z S_{i+1}^z) + \sum_{i=1}^N (h_x S_i^x + h_y S_i^y + w_i S_i^z) + J_p \sum_{i=1}^{N-2} S_i^z S_{i+2}^z \quad (2)$$

and choose the basis states to be products of eigenstates of the S_i^z operators. Here, S_i^a are the spin-1/2 operators for the spin at site i . The terms with strengths J_x , J_y , and J_z describe spin interactions, the terms with strengths h_x , h_y , and w_i represent a magnetic field, and we include the next-nearest neighbour term of strength J_p to avoid integrability. We take the interaction term in (1) to be $V_{\text{int}} = \vec{S}_N \cdot \vec{S}_{N+1}$.

It was shown in [39] that the rainbow state

$$|\psi_{\text{RB}}\rangle = 2^{-N/2} \bigotimes_{i=1}^N (|\uparrow, \uparrow\rangle_{i, 2N+1-i} + |\downarrow, \downarrow\rangle_{i, 2N+1-i}) \quad (3)$$

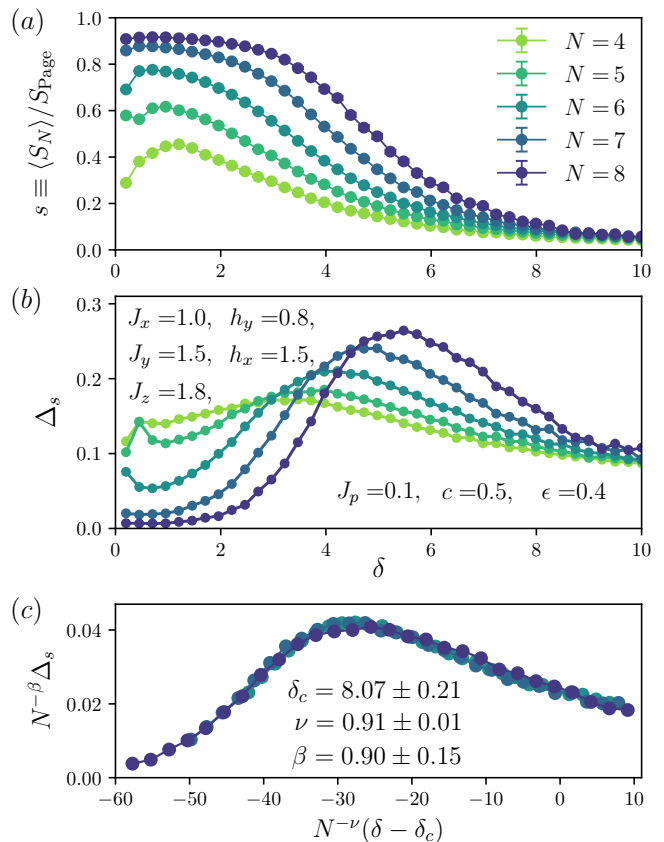


FIG. 1. (a) Disorder averaged half-chain entanglement entropy divided by the Page [4] value $S_{\text{Page}} = [2N \ln(2) - 1]/2$ for the eigenstate closest to the energy density $\epsilon = 0.4$ plotted against the disorder strength δ for different system sizes. The transition from thermal behavior at weak disorder to MBL behavior at strong disorder is seen. The number of disorder realizations is 10^4 for $N \in \{4, 5, 6\}$, 5000 for $N = 7$, and 1500 for $N = 8$. (b) The standard deviation of the half-chain entanglement entropy Δ_s computed for the same set of data shows a peak at the transition point. (c) The finite-size scaling collapse for Δ_s suggests that the transition happens at $\delta \sim 8$ for large systems.

is an exact eigenstate of H with energy $E_{\text{RB}} = c/4$. The rainbow state is a product of Bell states between pairs of spins on opposite halves of the system. The von Neumann entanglement entropy is $\ln(2)$ times the number of Bell pairs that are cut by the chosen bipartition, and hence most choices lead to volume law entanglement [39]. The maximal entanglement entropy is achieved for the half-chain bipartition.

We introduce disorder of strength δ by choosing w_i from a uniform distribution in the interval $[-\delta, \delta]$. The rainbow state is an exact eigenstate independent of the disorder realization. Disorder does, however, affect other states, driving an eigenstate transition from a thermal to an MBL behavior in Hamiltonians with local terms. We show in the following that the disorder indeed many-body localizes the system, except for a set of states near the rainbow state of measure zero. Unless stated oth-

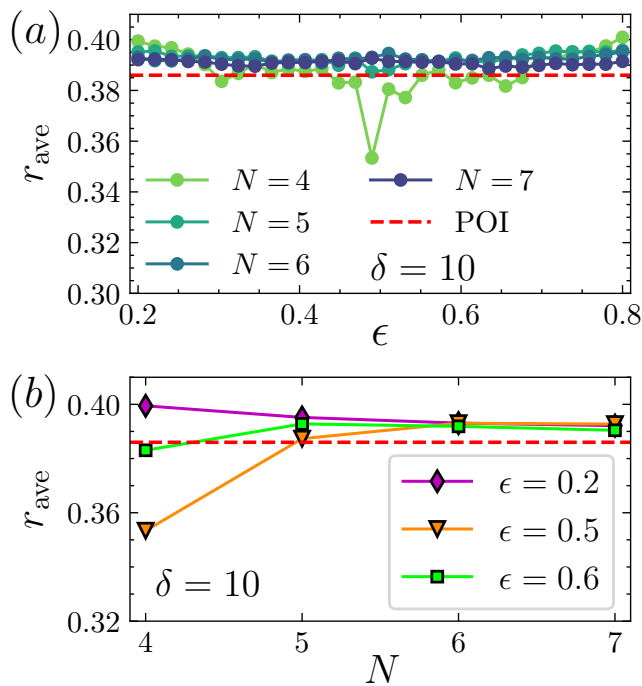


FIG. 2. (a) Adjacent gap ratio r_{ave} at strong disorder $\delta = 10$ computed for the 13, 50, 100, or 800 energy levels closest to the considered energy density for $N = 4, 5, 6,$ or 7 , respectively, and averaged over 3000 disorder realizations. As the system size $2N$ increases, r_{ave} gets close to the Poisson (POI) value, which signals that the majority of the states in the spectrum are many-body localized. (b) The same data, but plotted as a function of system size for different energy densities.

erwise, we take $J_x = 1$, $J_y = 1.5$, $J_z = 1.8$, $h_x = 1.5$, $h_y = 0.8$, $J_p = 0.1$, and $c = 0.5$ in the computations below. We do not expect the results to be specific to this choice of parameters. The values have been chosen in part to reduce the symmetry of the model and to have the rainbow state close to the middle of the spectrum. The computations for $N \leq 6$ are performed by employing full exact diagonalization. For $N > 6$, we use the shift-invert spectral transformation, implemented by PETSc [40, 41], SLEPc [42], and MUMPS [43] to perform Lanczos iteration on the transformed matrix via parallel sparse LU factorization as a direct solver.

Many-body localization—We first show that the disorder many-body localizes most of the states in the spectrum. We do this by computing the mean and variance of the half-chain entanglement entropy [44] and the level spacing statistics [5].

We first consider the half-chain von Neumann entanglement entropy $S_N = -\text{Tr}[\rho_N \ln(\rho_N)]$ of an exact eigenstate $|\psi\rangle$ of the system, where $\rho_N = \text{Tr}_{N+1:2N}(|\psi\rangle\langle\psi|)$ is the reduced density matrix obtained after tracing over the spins $N + 1$ to $2N$. When averaging the entanglement entropy over disorder realizations, we choose the state with energy density closest to a chosen value

in each realization. The energy density is defined as $\epsilon = (E - E_{\text{min}}^i)/(E_{\text{max}}^i - E_{\text{min}}^i)$, where E_{min}^i and E_{max}^i are the minimum and maximum energies in the spectrum of the i th disorder realization and E is the energy of the state $|\psi\rangle$.

In Fig. 1(a), we plot the mean of the entanglement entropy as a function of the disorder parameter δ for the state closest to the energy density $\epsilon = 0.4$. We have chosen this value to consider states close to the middle of the spectrum, while not being too close to the rainbow state, which for most disorder realizations has an energy density close to 0.5. For weak disorder, the mean entanglement entropy is comparable to the Page value [4], which signals thermal behavior. For strong disorder, the mean entanglement entropy is independent of system size, which signals MBL. The standard deviation of the entanglement entropy, plotted in Fig. 1(b), shows a peak at the transition point, and the finite-size scaling collapse in Fig. 1(c) suggests that the transition happens at $\delta \sim 8$ for large systems.

The level spacing statistics is another diagnostics to identify whether a system is MBL. Define the energy spacing $\Delta_n = E_{n+1} - E_n$ and the ratio $r_n = \min(\Delta_n, \Delta_{n+1})/\max(\Delta_n, \Delta_{n+1})$, where E_n is the n th energy in the spectrum, and let r_{ave} be the average of r_n over a selected part of the spectrum and over disorder realizations. Arguments from random matrix theory predict that $r_{\text{ave}} \approx 0.59$ for thermal states in systems with broken time reversal symmetry, while $r_{\text{ave}} \approx 0.386$ in MBL systems.

Figure 2 shows r_{ave} as a function of energy density and system size. When the system size increases, the Hilbert space dimension increases, and we hence also average over a larger number of states in the spectrum as detailed in the caption. It is seen that r_{ave} approaches the Poisson value $r_{\text{ave}} \approx 0.386$ for large system sizes, which signals that most of the states in the spectrum are many-body localized.

Highly entangled states—The entanglement entropy of the rainbow state is $N \ln(2)$ for the half-chain bipartition. Since the rainbow state remains unchanged upon introducing disorder, it has a high entropy compared to the many-body localized states, which are area law entangled. We now take a closer look at the behavior of the states in the spectrum that have energies close to the energy of the rainbow state.

Figure 3(a) shows the half-chain entanglement entropy as a function of disorder strength. To probe the states in the vicinity of the rainbow state, we here perform disorder averaging over states that have the same $n - n_{\text{RB}}^i$, where n labels the states in the spectrum from lowest to highest energy and n_{RB}^i is the n for the rainbow state for the i th disorder realization. The figure shows a narrow band of high entropy states. Crucially, this band is also present for disorder strengths for which the other states in the spectrum are many-body localized. Upon increasing energy, one hence finds a mobility edge followed by an inverted mobility edge. It is interesting to note that the

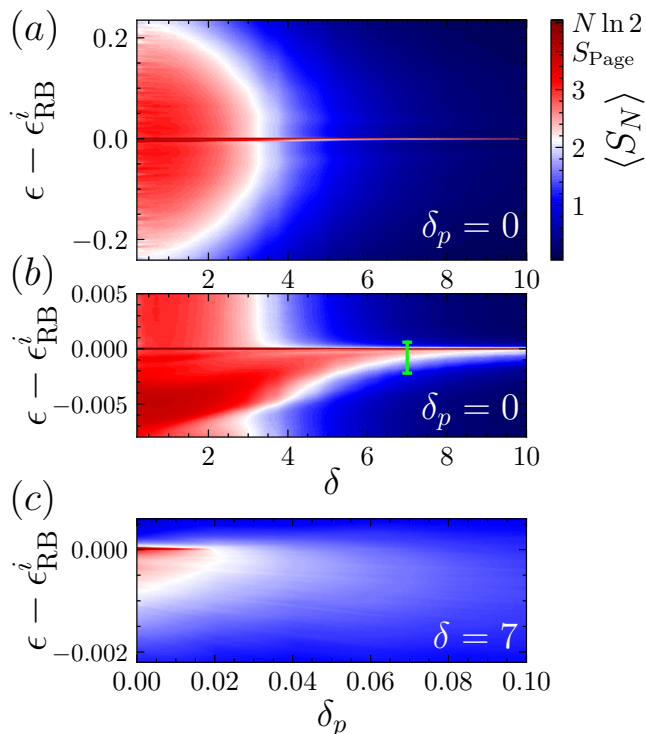


FIG. 3. (a) The disorder averaged half-chain entanglement entropy $\langle S_N \rangle$ as a function of disorder strength δ and energy density relative to the rainbow state $\epsilon - \epsilon_{\text{RB}}^i$ for $N = 6$. We average states with the same value of $n - n_{\text{RB}}^i$ over 2000 disorder realizations, where n_{RB}^i denotes the index of the rainbow state which lies at energy density $\epsilon_{\text{RB}}^i = (E_{\text{RB}} - E_{\text{min}}^i)/(E_{\text{max}}^i - E_{\text{min}}^i)$ for the i th disorder realization. The dark horizontal line at zero is produced by the rainbow state, and other highly entangled states are seen in its vicinity. Within the strongly disordered regime where the rest of the spectrum is many-body localized, these highly entangled states produce a mobility edge. (b) A zoom of panel (a) showing the band of high entropy states. Most of the high entropy states have energies below the rainbow state, but a few of them are at energies higher than the rainbow state. (c) $\langle S_N \rangle$ for a fixed $\delta = 7$ as a function of additional disorder of strength δ_p on the second half of the chain only. The high entropy states disappear for $\delta_p \approx \delta/300$. (The symmetric case, $\delta_p = 0$, also provides a magnified version of the mobility edges at the cut denoted by the short, vertical, green line in panel (b).)

entanglement entropy changes much faster with energy density when crossing the band of high entropy states than it does when crossing the white arc in the left half of the figure that separates the thermal region (red) from the MBL region (blue). We also note that the transition from high to low entropy when crossing the band of high entropy states is particularly sharp as seen in Fig. 3(b).

To count the number of high entropy states in the spectrum, we introduce a cutoff f_c and count how many states have an entropy higher than $S_c = f_c N \ln(2)$. This number is plotted as a function of system size for fixed disorder strength and different cutoffs in Fig. 4. It is seen

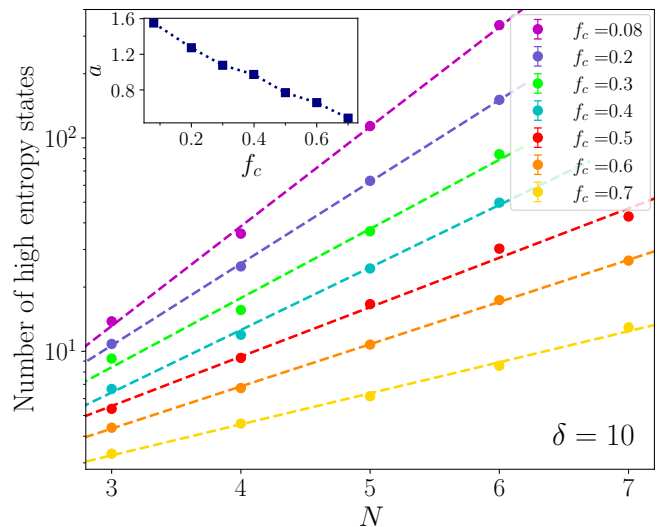


FIG. 4. Scaling of the number of atypical eigenstates with high entanglement entropy as a function of system size for $\delta = 10$. The number of atypical eigenstates with entropy higher than a certain cutoff value, $S_c = f_c N \ln(2)$, in each disorder realization, and this number is then averaged over 2000 disorder realizations for $N = 3, 4, 5, 6$ or 1090 for $N = 7$. For all considered f_c , the number of atypical eigenstates scales exponentially with N , and the dashed lines indicate the best fit with the function 2^{aN+b} . The inset shows a as a function of f_c . Note that $a < 2$ for all considered f_c , which means that the fraction of atypical states approaches zero for large system sizes.

that the number of high entropy states scales exponentially with system size, but the exponent is small enough that the fraction of high entropy states to the total number of states goes to zero in the large system limit.

Sensitivity to symmetry breaking—We test the stability of the observed behaviour to a perturbation which distinguishes between the two half-chains in the Hamiltonian (1), and thereby violates the symmetry underpinning the rainbow state. Concretely, we add further disorder $-w_i + \chi_i$ to the second half of the chain, i.e. sites $2N + 1 - i$, where χ_i is uniformly distributed within $[-\delta_p, \delta_p]$. We find, for $N = 6$ and $\delta = 7$ (Fig. 3(b)), that high entropy states are formed for $\delta_p \lesssim 0.02$, which is about 0.3% of δ .

Conclusion—We have demonstrated a scenario in which an inverted quantum many-body scar with volume law scaling of entanglement entropy is embedded in a spectrum of many-body localized states. The construction does not depend on the microscopic details of the Hamiltonian, except that a specific symmetry constraint needs to be obeyed. Similarly to many quantum scar models, the states in the vicinity of the scar state have modified entanglement compared to the remainder of the spectrum. The number of high entropy states scales exponentially with system size, but not as fast as the dimension of the Hilbert space. The high entropy states

thus form a narrow band in the spectrum, demarcated by sharp mobility edges. From our finite-size numerics, we cannot conclude whether the disorder strength at which the transition to MBL happens remains finite in the thermodynamic limit, but if it does, we expect the mobility edges to also remain. The sharp mobility edges over a broad range of disorder strengths in the finite systems may additionally be appealing for experiments and applications. We have also shown that the symmetry constraint does not need to be exactly obeyed to see inverted quantum many-body scarring.

Multiple exact volume law scars may be built by including further symmetries in the Hamiltonian [39] and this can lead to an interesting phase with multiple volume law states within a spectrum of MBL states. It would also be interesting to investigate the dynamics in

these multiple inverted scar models and study the late time behavior of some simple initial states.

ACKNOWLEDGMENTS

Acknowledgments—This work has been supported by Carlsbergfondet under Grant No. CF20-0658, by Danmarks Frie Forskningsfond under Grant No. 8049-00074B, by the UKRI Future Leaders Fellowship MR/T040947/1, and by the Deutsche Forschungsgemeinschaft under grants SFB 1143 (project-id 247310070) and the cluster of excellence ct.qmat (EXC 2147, project-id 390858490).

-
- [1] J. M. Deutsch, Quantum statistical mechanics in a closed system, *Phys. Rev. A* **43**, 2046 (1991).
 - [2] M. Srednicki, Chaos and quantum thermalization, *Phys. Rev. E* **50**, 888 (1994).
 - [3] R. Nandkishore and D. A. Huse, Many-body localization and thermalization in quantum statistical mechanics, *Annu. Rev. Condens. Matter Phys.* **6**, 15 (2015).
 - [4] D. N. Page, Average entropy of a subsystem, *Phys. Rev. Lett.* **71**, 1291 (1993).
 - [5] L. D'Alessio, Y. Kafri, A. Polkovnikov, and M. Rigol, From quantum chaos and eigenstate thermalization to statistical mechanics and thermodynamics, *Advances in Physics* **65**, 239 (2016).
 - [6] D. A. Abanin, E. Altman, I. Bloch, and M. Serbyn, *Colloquium: Many-body localization, thermalization, and entanglement*, *Rev. Mod. Phys.* **91**, 021001 (2019).
 - [7] J. Suntajs, J. Bonča, T. c. v. Prosen, and L. Vidmar, Ergodicity breaking transition in finite disordered spin chains, *Phys. Rev. B* **102**, 064207 (2020).
 - [8] J. Šuntajs, J. Bonča, T. c. v. Prosen, and L. Vidmar, Quantum chaos challenges many-body localization, *Phys. Rev. E* **102**, 062144 (2020).
 - [9] A. Morningstar, L. Colmenarez, V. Khemani, D. J. Luitz, and D. A. Huse, Avalanches and many-body resonances in many-body localized systems, *Phys. Rev. B* **105**, 174205 (2022).
 - [10] M. Schreiber, S. S. Hodgman, P. Bordia, H. P. Lüschen, M. H. Fischer, R. Vosk, E. Altman, U. Schneider, and I. Bloch, Observation of many-body localization of interacting fermions in a quasirandom optical lattice, *Science* **349**, 842 (2015).
 - [11] M. Serbyn, D. A. Abanin, and Z. Papić, Quantum many-body scars and weak breaking of ergodicity, *Nature Physics* **17**, 675 (2021).
 - [12] S. Moudgalya, B. A. Bernevig, and N. Regnault, Quantum many-body scars and Hilbert space fragmentation: a review of exact results, *Rep. Prog. Phys.* **85**, 086501 (2022).
 - [13] A. Chandran, T. Iadecola, V. Khemani, and R. Moessner, Quantum many-body scars: A quasiparticle perspective, *Annual Review of Condensed Matter Physics* **14**, 443 (2023).
 - [14] S. Moudgalya, S. Rachel, B. A. Bernevig, and N. Regnault, Exact excited states of nonintegrable models, *Phys. Rev. B* **98**, 235155 (2018).
 - [15] C. J. Turner, A. A. Michailidis, D. A. Abanin, M. Serbyn, and Z. Papić, Quantum scarred eigenstates in a Rydberg atom chain: Entanglement, breakdown of thermalization, and stability to perturbations, *Phys. Rev. B* **98**, 155134 (2018).
 - [16] M. Schecter and T. Iadecola, Weak Ergodicity Breaking and Quantum Many-Body Scars in Spin-1 XY Magnets, *Phys. Rev. Lett.* **123**, 147201 (2019).
 - [17] T. Iadecola and M. Schecter, Quantum many-body scar states with emergent kinetic constraints and finite-entanglement revivals, *Phys. Rev. B* **101**, 024306 (2020).
 - [18] S. Chattopadhyay, H. Pichler, M. D. Lukin, and W. W. Ho, Quantum many-body scars from virtual entangled pairs, *Phys. Rev. B* **101**, 174308 (2020).
 - [19] S. Moudgalya, A. Prem, R. Nandkishore, N. Regnault, and B. A. Bernevig, Thermalization and its absence within Krylov subspaces of a constrained Hamiltonian, in *Memorial Volume for Shoucheng Zhang* (World Scientific, 2021) pp. 147–209.
 - [20] Z. Yao, L. Pan, S. Liu, and H. Zhai, Quantum many-body scars and quantum criticality, *Phys. Rev. B* **105**, 125123 (2022).
 - [21] N. Shiraishi and T. Mori, Systematic Construction of Counterexamples to the Eigenstate Thermalization Hypothesis, *Phys. Rev. Lett.* **119**, 030601 (2017).
 - [22] D. M. Basko, I. L. Aleiner, and B. L. Altshuler, Metal-insulator transition in a weakly interacting many-electron system with localized single-particle states, *Annals of physics* **321**, 1126 (2006).
 - [23] I. Mondragon-Shem, A. Pal, T. L. Hughes, and C. R. Laumann, Many-body mobility edge due to symmetry-constrained dynamics and strong interactions, *Phys. Rev. B* **92**, 064203 (2015).
 - [24] W. De Roeck, F. Huveneers, M. Müller, and M. Schiulaz, Absence of many-body mobility edges, *Phys. Rev. B* **93**, 014203 (2016).
 - [25] Y.-T. Hsu, X. Li, D.-L. Deng, and S. Das Sarma, Machine Learning Many-Body Localization: Search for the Elusive Nonergodic Metal, *Phys. Rev. Lett.* **121**, 245701 (2018).

- (2018).
- [26] N. S. Srivatsa, R. Moessner, and A. E. B. Nielsen, Many-Body Delocalization via Emergent Symmetry, *Phys. Rev. Lett.* **125**, 240401 (2020).
- [27] M. Iversen, N. S. Srivatsa, and A. E. B. Nielsen, Escaping many-body localization in an exact eigenstate, *Phys. Rev. B* **106**, 214201 (2022).
- [28] W. Cottrell, B. Freivogel, D. M. Hofman, and S. F. Lohkhande, How to build the thermofield double state, *Journal of High Energy Physics* **2019**, 1 (2019).
- [29] S. Biswas, D. Banerjee, and A. Sen, Scars from protected zero modes and beyond in $U(1)$ quantum link and quantum dimer models, *SciPost Physics* **12**, 148 (2022).
- [30] A. Russomanno, M. Fava, and R. Fazio, Weak ergodicity breaking in Josephson-junction arrays, *Phys. Rev. B* **106**, 035123 (2022).
- [31] D. J. Luitz, N. Laflorencie, and F. Alet, Many-body localization edge in the random-field Heisenberg chain, *Phys. Rev. B* **91**, 081103(R) (2015).
- [32] D. Tong, Lectures on the quantum Hall effect (2016), arXiv:1606.06687.
- [33] R. Nandkishore and A. C. Potter, Marginal Anderson localization and many-body delocalization, *Phys. Rev. B* **90**, 195115 (2014).
- [34] S. Banerjee and E. Altman, Variable-Range Hopping through Marginally Localized Phonons, *Phys. Rev. Lett.* **116**, 116601 (2016).
- [35] A. C. Potter and R. Vasseur, Symmetry constraints on many-body localization, *Phys. Rev. B* **94**, 224206 (2016).
- [36] G. Vitagliano, A. Riera, and J. I. Latorre, Volume-law scaling for the entanglement entropy in spin-1/2 chains, *New Journal of Physics* **12**, 113049 (2010).
- [37] G. Ramírez, J. Rodríguez-Laguna, and G. Sierra, From conformal to volume law for the entanglement entropy in exponentially deformed critical spin 1/2 chains, *J. Stat. Mech.* **2014**, P10004 (2014).
- [38] G. Ramírez, J. Rodríguez-Laguna, and G. Sierra, Entanglement over the rainbow, *J. Stat. Mech.* **2015**, P06002 (2015).
- [39] C. M. Langlett, Z.-C. Yang, J. Wildeboer, A. V. Gorshkov, T. Iadecola, and S. Xu, Rainbow scars: From area to volume law, *Phys. Rev. B* **105**, L060301 (2022).
- [40] S. Balay, S. Abhyankar, M. Adams, P. Brune, K. Buschelman, L. Dalcin, W. Gropp, B. Smith, D. Karpeyev, D. Kaushik, *et al.*, *Petsc users manual revision 3.7*, Tech. Rep. (Argonne National Lab.(ANL), Argonne, IL (United States), 2016).
- [41] S. Balay, W. D. Gropp, L. C. McInnes, and B. F. Smith, Efficient management of parallelism in object oriented numerical software libraries, in *Modern Software Tools in Scientific Computing*, edited by E. Arge, A. M. Bruaset, and H. P. Langtangen (Birkhäuser Press, 1997) pp. 163–202.
- [42] V. Hernandez, J. E. Roman, and V. Vidal, SlepC: A scalable and flexible toolkit for the solution of eigenvalue problems, *ACM Trans. Math. Softw.* **31**, 351 (2005).
- [43] P. R. Amestoy, A. Guermouche, J.-Y. L’Excellent, and S. Pralet, Hybrid scheduling for the parallel solution of linear systems, *Parallel Computing* **32**, 136 (2006).
- [44] J. A. Kjäll, J. H. Bardarson, and F. Pollmann, Many-Body Localization in a Disordered Quantum Ising Chain, *Phys. Rev. Lett.* **113**, 107204 (2014).